VOL. 18, NO. 22, NOVEMBER 2023 ISSN 1819-6608
ARPN Journal of Engineering and Applied Sciences

www.arpnjournals.com

IMPACT OF THERMAL DIFFUSION AND DIFFUSION-THERMAL EFFECTS ON MHD MAXWELL FLUID SUBJECT TO NEWTONIAN HEAT AND MASS CONDITIONS OVER A STRETCHING CYLINDER

M. Sreedhar Babu[1] and Velpula Venkata Ramana[2]
[1]Department of Applied Mathematics, Yogi Vemana University, Kadapa, Andhara Pradesh, India
[2]Department of Mathematics, Faculty of Mathematics, Rajiv Gandhi University of Knowledge Technologies, Srikakulam, Andhra Pradesh, India
E-Mail: msreedharyvu@gmail.com

ABSTRACT

Current research's main focus is to incorporate the novel idea of Newtonian flux condition in MHD stretching flow of Maxwell liquid with Stefan blowing. An analysis is done to explore the heat and mass transfer characteristics of MHD Maxwell fluid towards a stretching cylinder, including thermal diffusion and diffusion-thermal energy implications in the presence of activation energy. Polar coordinates (z, r) in the shape of a cylinder are used to model the issue. To convert controlling PDEs into ODEs, similarity the variables are used. The governing equations of motion that result are tackled via the notorious R-K 4th order approach. Through graphical portrayal, the impacts of various factors, including curvature, magnetics, Stefan blowing, reaction, and activation energy parameters, are studied. Furthermore, the validation of numerical findings is prepared by benchmarking with previously determined limiting conditions, and we launch a wonderful communication with these results.

Keywords: stefan blowing, activation energy, soret effect, dufour effect, brownian motion.

Manuscript Received 22 July 2023; Revised 12 January 2024; Published 30 January 2024

INTRODUCTION

A rate-type model was put out by Maxwell [1], and it is renowned for its viscoelastic implementation and stress-relaxation prediction. A fascinating area of research for mathematicians, physicists, and engineers is the study of stretching surfaces. Problems in industrial sectors, including as aerodynamics, petroleum, and pharmaceutical processes, are also significantly addressed by the non-Newtonian Maxwell model. To simulate the Maxwell MHD flow and shooting method, Mukhopadhyay [2] used the boundary layer theory. The thermal conductivity two-phase media for the Maxwell fluid was identified by Yang *et al*. [3]. They found reduced conduction because to stretchiness-induced insulating holes. Irfan *et al*. [5] utilized the HAM for Maxwell fluid with the consideration of source/sink, whereas Ramzan *et al*. [4] explored convective Maxwell flow with the Dufour impression. Recently, Loganathan [6] used double diffusive towards a detested stretchy surface Cattaneo-Christov model to articulate how heat radiation affects MHD Maxwell fluid. With the aid of the Cattaneo-Christov model and a chemical reaction, Sajid *et al.*'s [7] investigation into the heat and mass transfer characteristics of an upper convective slip flow of MHD Maxwell fluid over porous media. The impact of thermophoresis and Dufour-Soret effects on a Maxwell fluid in a Darcy medium was established by Nuwairan *et al*. [8] by incorporating thermal radiation and a heat source across a rotating disc.

The effect of fluid flow across a stretched cylinder has been investigated using a variety of experimental, analytical, and computational processes. The flow analysis of a stretching cylinder has many real-world applications in engineering and business, such as cord illustration, spinning metal, piping, metallurgical extrusion methods, refinement of crude oil, production of elastic, glaze of cylinder-shaped cords and crust, and so on. By stretching a cylinder, Crane [9] examined the flow. Wang [10] then granted the constant viscous liquid flow in an ambient liquid that was at rest outside to a stretched hollow cylinder. Later, Wang and Ng [11] discussed the impact of a stretched cylinder in slip flow. This investigation established that slip negatively affects shear stress and velocity. Markin *et al* [12] took into account flow and heat transfer estimations with stagnation points generated by cylinder stretching/shrinking. This study demonstrated that a high curvature parameter increases the quantity of heat transmission at the surface. By stretching a cylinder, Hayat *et al*. [13] investigated the radiative flow of a magneto Eyring-Powell micro liquid. Mathematically, Rehman *et al.* [14] examined the influence of thermally stratified and Magneto hydrodynamics (MHD) on Casson liquid across a stretched cylinder. By integrating convective boundary conditions, Islam *et al*. [15] investigated the effects of joule heating on the spinning motion of mixed convective Maxwell liquid flow across a bi-directional stretched cylinder together with thermal radiation and a heat source. Temperature and concentration gradients produce mass and energy flows, respectively. Thermal-diffusion (Soret effect) is caused by temperature gradients, whereas the Dufour and Soret effects are caused by concentration gradients. When there are variations in the flow's densities, the significance of these factors becomes very apparent. Numerous real-world applications, including those in the

geosciences, waste management, cooling applications, steel industries, heat exchangers, and chemical engineering, experience these impacts. Also Reactor safety, combustion flames, solar collectors, and building energy conservation are all areas where the Soret and Dufour effects are applied. The diffusion-thermo or Dufour influence of the concentration gradient's heat flow is indicated. In the meanwhile, thermo-diffusion or Soret impacts are used to describe the mass flow caused by temperature gradient. The non-dimensional concentration equation and the energy equation, respectively, contain the Soret and Dufour terms. The magnitude order of the Soret and Dufour impacts is typically not taken into account since it is smaller than the impact determined by Fourier and Fick's equations. However, when a species is present at a fluid's surface that has a lower density than the surrounding fluid, the effects are taken into account. Numerous academics have examined the effects of Soret and Dufour on flow in various geometries. The hydromagnetic flow of Casson fluid on a stretched surface with the effects of Soret and Dufour was investigated by Hayat *et al*. Mahdy [17] investigated the influence of Soret and Dufour effects on the flow of casson fluid across a stretched cylinder by incorporating suction (blowing).In the context of MHD, radiative heat transfer, Soret and Dufour, Pal *et al*. [18] addressed the mixed convection flow of nanofluid across a nonlinear stretching and shrinking surfaces. Khan *et al.'s* [19] investigation of the flow of a Jeffrey fluid with HAM through a stretched cylinder with Soret and Dufour effects is also worth mentioning. The influence of Soret and Dufour on the nanofluid flow through a stretched cylinder along with triple stratification was examined by Jagan *et al*. [20, 21]. Manoj *et al*. [22] discussed the impact of Soret and Dufour on the flow of nano fluid through a stretched cylinder combined with heat radiation in the presence of Stefan blowing. Ahmed *et al.* [23] acquired Keller box solution for a third-grade fluid to investigate the effects of Soret and Dufour aspects across a stretched cylinder coupled with thermal radiation.

The blowing effect is brought on by the collective movement of particles or nanoparticles from one location to another. Evaporation, absorption, combustion, materials synthesis, and distillation all depend on mass transfer. There are several uses for Stefan blowing, also known as wall injection, in engineering systems, including drying operations when it has perforated. Spalding was the first to research the concept of wall injection, which is shown in the Stefan problem [24]. Fang and Jing [25] investigated how heat flowed through a stretchy plate while taking wall injection into consideration. Alamri *et al*. [26] examined the impact of the Stefan bowling effect on the Poiseuille flow of nanofluids while accounting for the slip effect of a porous media. Through the use of the Buongiorno model, Amirsom *et al*. [27] demonstrated the impact of Stefan blowing on the stream of fluid passing a needle. Williamson fluid flow across porous walls was studied by Yusuf *et al*. [28] using the differential transformation approach while accounting for the slip effect and chemical interactions. The Stefan blowing effect on the radiative stream of micro liquid passing a plate was discussed by Ali *et al*. [29].

Because it has several industrial applications in nuclear reacting cooling, geothermal reservoirs, chemical engineering, and thermal oil recovery, the mass transfer analysis under the combined influence of activation energy and chemical reaction obtained a spectacular response. The deployment of reactant species and their synthesis at varied speeds within the mass transfer of nanofluid may be used to analyse the relationship between mass transfer and chemical reaction, which is generally highly important. These uses have led several researchers to investigate how these effects affect different liquid streams with diverse geometry. Zaib *et al*. [30] investigated how the second law affected the EMHD Casson fluid when it approached a wedge in presence activation energy. The impact of activation energy on the flow of suspended AA7072/AA7075 nanofluids over three various geometries was investigated by Rekha *et al.* By introducing the zero mass flux condition, Reddy *et al*. [32] investigated the impact of activation energy on the MHD second-grade fluid flow across a curved stretched surface. A mathematical model for wall jet (WJ) flow by Khan *et al.* [33] was composed of a colloidal combination of SAE50 and zinc oxide nanoparticles in the presence of activation energy. In the presence of activation energy, Khan et al.'s research [34] explored the bio-convective flow of Maxwell nanoparticles through a stretched and rotating cylinder in a porous media. The MHD flow of chemically reactive Prandtl nanofluid containing microbe in presence of activation energy was described by Zafar *et al*. [35]. Between two endlessly revolving horizontal channels, Zeeshan *et al.'s* [36] analysis of the nanofluid flow included activation energy.

Our goal in this effort is to assess how Newtonian heat and mass processes interact with Maxwell fluid as it moves toward a stretched cylinder. Only Newtonian heating of heat transfer has been employed in previous studies to study the characteristics of various fluid models under varied aspects and flow geometries. Here, we took into account the Newtonian mass requirement for the non-Newtonian liquid's stretching flow behaviour. The Stefan blowing condition and the activation energy issue were also covered. The problem's numerical solution is obtained by combining the Runge-Kutta and firing techniques. In two situations, the results are presented as charts and tables. An analysis of the prior research is conducted to confirm the accuracy of our inquiry, and all findings are discovered to be in commendable agreement.

MATHEMATICAL FORMULATION

Think about a smooth, 2D MHD Maxwell fluid flow that is being affected by a stretched, a_o radius cylinder that is encased in a porous substance. The cylinder's axis is subjected to a normal magnetic field. Where u_p is the reference velocity and l is the particular length, the cylindrical object is stretched with velocity $u_p z / l$ along the $z-$ direction. Let's assume that the $r-$

axis is constrained to the radial direction and that the $z-$ axis is considered to be next to the cylinder's axis, as illustrated in figure.1. For heat and mass transmission methods, thermal radiation, Brownian and thermophoresis characteristics are presented. A first-order homogeneous chemical reaction is considered to occur in the flow while also accounting for the concentration of diffusing species, thermal diffusion, and diffusion-thermal energy effects. The effects of Stefan blowing are also taken into account. Chemical reactions and activation energy are also included to analyze the nature of mass and heat transport. The governing equations for this physical scenario are based on the standard balancing laws of mass, linear momentum, energy, and mass diffusion adjusted to take into consideration the physical processes indicated above. Following are the equations for the Maxwell nanofluid model's estimated boundary layer in natural representation:

$$(ru)_x+(rv)_r=0 \tag{1}$$

$$u w_r+w w_z+\lambda_1\left[w^2 w_{zz}+u^2 w_{rr}+2wuw_{zr}\right]=\vartheta\left[w_{rr}+\frac{w_r}{r}\right] -\frac{\sigma B_o^{\,2}}{\rho}\left[\lambda_1 u w_r+w\right] \tag{2}$$

$$uT_r+wT_z=\alpha\left[T_{rr}+\frac{T_r}{r}\right]+\tau\left[D_B C_r T_r+\frac{D_T}{T_\infty}T_r^2\right]+\frac{D_B k_T}{C_s C_p}\left[C_{rr}+\frac{C_r}{r}\right] \tag{3}$$

$$uC_x+vC_r=D_B\left[C_{rr}+\frac{C_r}{r}\right]+\frac{D_B k_T}{T_m}\left[T_{rr}+\frac{T_r}{r}\right] -k_s^2\left(\frac{T}{T_\infty}\right)^s e^{-\frac{E_a}{k_1 T}}(C-C_\infty) \tag{4}$$

With the boundary conditions:

$$u=u_w,\ v=\frac{-D_B}{1-C_w}\frac{\partial C}{\partial r},\quad \frac{\partial T}{\partial r}=-h_t T,\ \frac{\partial C}{\partial r}=-h_c C,$$

At $r=a_o$ (5)

$$u\to 0,\ T\to T_\infty,\ C\to C_\infty \ \text{ As } r\to\infty \tag{6}$$

Here ϑ,ρ,k,c_p stands for kinematic viscosity, density, thermal conductivity, and specific heat at constant pressure and $\alpha=k/\rho c_p$ Stands for thermal diffusivity. D_B *and* D_T Stands for Brownian diffusion and thermophoresis diffusion coefficients, respectively,

On employing $w=\frac{u_p z}{l}G'(\zeta)$,

$$u=-\frac{a_o}{r}\sqrt{\frac{u_p}{l}}\,\vartheta\, G(\zeta),\ \theta(\zeta)=\frac{T-T_\infty}{T_\infty},$$

$$\Phi(\zeta)=\frac{C-C_\infty}{C_\infty} \text{ and } \zeta=\sqrt{\frac{u_p}{l\vartheta}}\left(\frac{r^2-a_o^{\,2}}{2a_o}\right)$$ ([53], [54]) the equation of continuity (2) is fulfilled and the equations from (3) to (7) take the following form.

$$(1+2\zeta\alpha_c)G'''+2\alpha_c G''-G'^2+GG''+2\beta_p GG'G''-\beta_p G^2G''' -\frac{\alpha_c\beta_p}{(1+2\zeta\alpha_c)}G^2G''-M_p[G'-\beta_p GG'']=0 \tag{7}$$

$$\left[(1+2\zeta\alpha_c)\right]\theta''+2\alpha_c\theta'+\Pr G\theta'+(1+2\zeta\alpha_c)\Pr Nb_p\theta'\Phi' +(1+2\zeta\alpha_c)\Pr Nt_p\theta'^2+\Pr Du_p\left[(1+2\zeta\alpha_c)\Phi''+2\alpha_c\Phi'\right]=0 \tag{8}$$

$$(1+2\eta\alpha)\Phi''+2\alpha\Phi'+Sc\, f\Phi'-\sigma Sc(1+\delta\theta)^s e^{-\frac{E}{1+\delta\theta}}\Phi +Sc\, Sr\left[(1+2\eta\alpha)\theta''+2\alpha\theta'\right]=0 \tag{9}$$

$$G(0)=\frac{sb_p}{Sc}\Phi'(0),\ G'(0)=1,$$

$$\theta'(0)=-\gamma_1(1+\theta(0)),\ \Phi'(0)=-\gamma_2(1+\Phi(0)) \tag{10}$$

$$G'(\infty)=0,\ \theta(\infty)=0,\ \Phi(\infty)=0 \tag{11}$$

The values of the parameters which are raised in the equations (7) to (11)

$$\Pr=\frac{\vartheta}{\alpha},\quad \alpha_c=\left(\frac{l\vartheta}{u_p a_o^{\,2}}\right)^{\frac{1}{2}},\quad M=\frac{\sigma B_0^2 l}{\rho u_p},$$

$$\beta_p=\frac{\lambda_1 u_p}{l}$$

$$Nb_p=\frac{\tau D_B C_\infty}{\vartheta}\quad Du_p=\frac{D_B k_T C_\infty}{C_s C_p T_\infty}\ Sc=\frac{v}{D_B},$$

$$Sr_p=\frac{D_B k_T T_\infty}{T_m\vartheta C_\infty}\ Sb_p=\frac{C_\infty}{1-C_\infty} \tag{12}$$

Skin Friction Coefficient

$$C_f=\frac{\tau_w}{\rho u_w^2}==\mathrm{Re}_z^{\frac{-1}{2}}\ f''(0) \tag{13}$$

Nusselt Number:

$$Nu_z=\frac{zq_w}{k(T_w-T_\infty)},\ q_w=-k\frac{\partial T}{\partial r}\Big|r=a_o\ ,\quad Nu_z\,\mathrm{Re}_z^{\frac{-1}{2}}=-\theta'(0) \tag{14}$$

Sherwood Number

$$Sh_z = \frac{zq_m}{D_B(C_w - C_\infty)},\ J_m = -D_B \frac{\partial C}{\partial r}\bigg| r = a_o\ ,\quad Sh_z \,\mathrm{Re}_z^{\frac{-1}{2}} = -\phi'(0) \quad (15)$$

Solution Procedure

Using the well-known R-K 4th order together with shooting technique, equations (7) through (11) are numerically analyzed. With this system, it is possible to select a workable solution for the flow parameters. To solve two-point boundary value issues, single order differential equations are used. The missing initial constraints are additionally assumed using the shooting method. Then, using R-K 4th order application, the resulting one is integrated.

Tables 1-4 are used to compare the analysis of recent work with readily available information. These tables show the outcomes of several previous studies along with the findings of the current study using the R-K 4th order approach. This comparison demonstrates high compatibility criteria. Using the shot technique, the skin friction coefficient and Nusselt number findings are compared when subjected to various varied flow characteristics.

RESULTS AND DISCUSSIONS

A study is conducted to investigate the thermal and thermal-energy impacts of thermal diffusion and diffusion-thermal energy effects in the presence of activation energy and Stefan blowing as they relate to the heat and mass transport characteristics of MHD Maxwell fluid towards a stretched cylinder. To solve the resultant governing differential equations, the well-known R-K 4th order approach is used.

Complete numerical computations for various parameters on velocity, temperature, and concentration profiles are available in this segment. The findings of the physical interpretation are displayed, examined, and debated utilising the graphical representations. In every graph, physical parameters for the whole numerical simulation are presented.

The effect of the curvature parameter α_c on the velocity component, liquid temperature, and Maxwell liquid concentration is shown in Figures 2(a), (b), and (c). According to reports, when α_c increases physically, the radius of curvature reduces, reducing the region where the cylinder interacts with the liquid while the Maxwell liquid velocity, temperature, and concentration fields grow. As a result, the resistance provided by the outside decreases and Maxwell liquid velocity rises. It is also observed that larger values of α_c result in an increase in the boundary layer's temperature as well as its associated thermal thickness. As a result, the temperature of the Maxwell nano liquid rises and the heat transmission is reduced.

The effect of the Maxwell parameter β_p on the velocity component, liquid temperature, and Maxwell liquid concentration is shown in Figures 3(a), (b), and (c). Figure-3a demonstrates that as β_p is increased, the velocity field drops because β_p causes resistance to the flow field. Figures 3b and 3c, however, illustrate the opposing behavior for heat and mass transmission. With rising Maxwell parameter values, the system's energy rises. Physically, the deformation of viscoelastic fluids is represented by β_p. The stress relaxation phenomena grows as β_p values rise, hardening the material under study, causing the gap between fluid particles to close. The velocity profile falls as a result and deformation takes more time to be sustained. Furthermore, the thermal conductivity of the fluid improves simultaneously, which eventually boosts the heat and mass transport phenomenon.

The velocity component, liquid temperature, and Maxwell liquid concentration are all affected by the magnetic parameter M_p, as shown in Figures 4(a), (b), and (c). Higher values of M_p intensify the Lorentz/electromagnetic force caused by the external magnetic field, which creates resistance to fluid flow. As a result, as M_p is increased, the velocity field diminishes. However, this force causes more fluid particle collisions, which dramatically raises the temperature and mass distribution. Figures 4b and 4c illustrate this result.

Stefan's blowing parameter, Sb_p, is shown in Figures 5(a), (b), and (c), which show how it affects velocity, temperature, and concentration profiles. As seen in Figure-5a, increased Stefan blowing causes the velocity profile to grow. The temperature and concentration profiles accelerated as a result of Stefan's increased wind speed and were carried farther from the surface to reach ambient temperature and ambient concentration. In response, the temperature and concentration profiles rise, as seen in Figures 5b and 5c.

The effects of thermophoresis (Nt_p) and Brownian motion (Nb_p) on the temperature and concentration distribution of Maxwell liquids are depicted in Figures 6(a, b) and 7(a, b). For escalating values of Nt_p and Nb_p on both distributions, same behavior is found. Physically, greater values of Nt_p raise the liquid temperature because the difference in temperature between the wall and the reference temperature grows. On the other hand, Nb_p is an ad hoc grouping of molecules that intensifies and improves the temperature field. Although the concentration of the Maxwell liquid implies that the intensifying values of Nt_p and Nb_p function differently.

Dufour parameter Du_p has an impact on temperature and concentration profiles, as seen in Figures 8a and 8b. It may

be inferred from Figure-8a that rising Du_p values also raise the temperature. Figure-8b illustrates a decrease in concentration by enhancing Du_p. Convection velocity increases due to the combined effects of heat and concentration while Du_p is physically rising. As a result, concentration decreases as temperature rises.

Sr_p has an impact on temperature and concentration profiles, as seen in Figures 9a and 9b. We may infer from figure 9a that a decrease in temperature is caused by rising Du_p values. For the enhancing values of Sr_p, the concentration distribution field in figure 9b is enhanced. Due to the thermal gradients created by the increasing values of Sr_p, more mass fluxes have been generated, resulting in this condition.

Prandtl number $\Pr$'s impact on the temperature field is seen in Figure-10. As $\Pr$ increases, the liquid's specific heat capacity increases, which reduces the fluid's thermal diffusivity because heat transfer slows fluid movement. As a result, the temperature field and heat transfer rate both drop.

Figures 11-12 show, respectively, how $\gamma_1 \text{ and } \gamma_2$ an impact has on temperature and concentration profiles. The increasing functions at both points 1 and 2 are temperature and concentration. Actually, h_t is a prerequisite for the thermal conjugate parameter γ_1. More mass and heat are transferred from heated to cold surfaces as a result of larger $\gamma_1 \text{ and } \gamma_2$ and corresponding increases in h_t and h_c. The liquid's concentration and temperature are raised as a result.

Schmidt number Sc's effect on concentration is seen in Figure-13. Given that Sc is a function of both momentum and mass diffusivity, when the diffusion ratio increases to 1, 2, 3, and 5, momentum diffusion takes precedence over mass diffusion. As a result, mass transportation declines.

Reaction parameter (σ) and activation energy parameter (E) effects on concentration profiles are shown in Figures 14 and 15. With increasing (σ) values in every example, a considerable decline in concentration profiles is seen. The Arrhenius expression grows when (σ) values do, which eventually harms the chemical process. Because of this, the concentration profiles decline. Figure-15 shows how the concentration profiles are affected by Energy Activation Number (E). The concentration profiles have been shown to rise when (E) values rise. Utilizing activation energy is more effective at speeding up the reaction and hence raising concentration. With an increase in (E) values, the Arrhenius expression deviates, causing the development of the relational chemical reaction and an increase in the concentration profiles. The reduced reaction rate caused by the phenomena of low temperature and higher activation energy slows the chemical process. The concentration rises in this manner.

CONCLUSIONS

The features of MHD Maxwell fluid's mass and heat transport are investigated about a stretched cylinder. To solve the resultant governing differential equations, the well-known R-K 4th order approach is used. Below are the key takeaways from the current investigation.

a) The influence of curvature parameter α_c on velocity component, temperature and concentration is the same
b) Velocity exhibits decreasing nature for increasing values of β_p, M_p
c) The influence of Stefan blowing parameter Sb_p on velocity component, temperature and concentration is the same
d) Temperature exhibits upsurge behavior for increasing values of $\beta_p, M_p, Nb_p, Nt_p \text{ and } \gamma_1$ and a reverse nature is detected for $Sr_p \text{ and } \Pr$
e) Concentration exhibits upsurge behavior for increasing values of $Sr_p, E \text{ and } \gamma_2$ and a reverse nature is detected for $Nb_p, Nt_p, Du_p \text{ and } \sigma$.

Table-1. Comparative study Skin Friction Coefficient with the existing reports for distinct values of β_p when $\alpha_c = 0$.

β_p	[37]	[38]	[39]	[40]	[45]	Present Outcomes
0	1.000000	0.999978	1.000000	1.0000000	1.000000	1.000000
0.2	1.051948	1.051945	1.051889	1.0518890	1.051556	1.051889
0.4	1.101850	1.101848	1.101903	1.1019035	1.101603	1.101903
0.6	1.150163	1.150160	1.150137	1.1501374	1.150356	1.150137
0.8	1.196692	1.196690	1.196711	1.1967114	1.196711	1.196712
1.0	----	----	----	----	1.241722	1.241753
1.2	1.285257	1.285253	1.285363	1.2853630	1.285355	1.285366

Table-2. Comparative study Skin Friction Coefficient with the existing reports for distinct values for M_p when $\alpha_c = 0 = \beta_p$.

M_p	[41]	[42]	[43]	[44]	[45]	Present Outcomes
0.5	1.1180	----	1.118034	1.224745	1.224742	1.224745
1.0	----	1.41421	1.414214	1.414213	1.414213	1.414214
1.5	----	----	----	----	1.581136	1.581139
2.0	----	----	----	----	1.732045	1.732051
5.0	----	2.44948	2.449483	2.449474	2.446251	2.449490

Table-3. Numerical data for Nusselt Number with the existing reports for distinct Pr values.

Pr	[46]	[47]	[48]	[49]	Present Outcomes
0.72	0.4631	0.4617	0.46315	0.4631	0.463145
1	0.5820	0.5801	0.58199	0.5820	0.581978
3	1.1652	1.1599	1.16523	1.1652	1.165253
10	2.3080	2.2960	2.30796	2.3080	2.308025
100	7.7657	----	7.76536	7.7657	7.765899

Table-4. Numerical data for Nusselt Number with the existing reports for distinct Pr values.

Pr	[50]	[51]	[52]	Present Outcomes
0.07	0.0663	0.0656	0.0656	0.065605
0.2	0.1691	0.1691	0.1691	0.169089
0.7	0.4539	0.4539	0.4539	0.453917
2	0.9113	0.9114	0.9114	0.911361
7	1.8954	1.8954	1.8905	1.895420
20	3.3539	3.3539	3.3539	3.353935
70	6.4621	6.4622	6.4622	6.462313

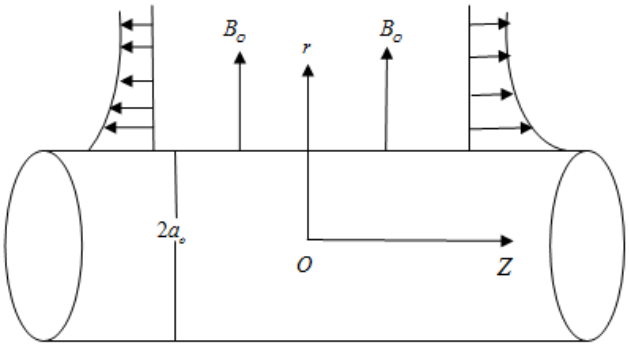

Figure-1. Flow configuration.

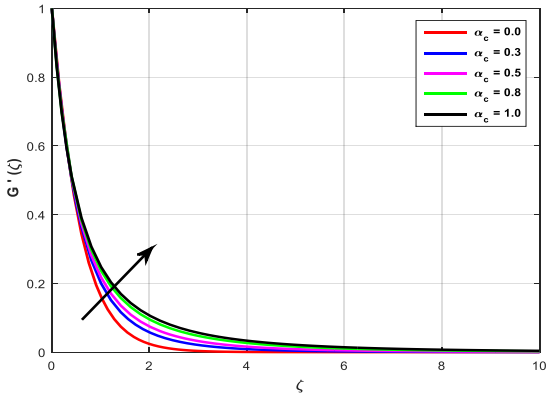

Figure-2a. Variations in $G'(\zeta)$ caused by α_c.

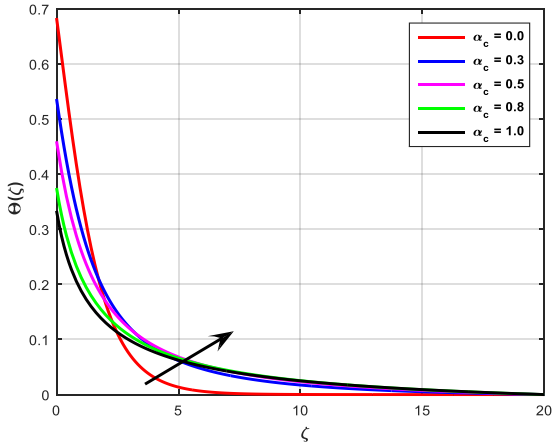

Figure-2b. Variations in $\theta(\zeta)$ caused by α_c.

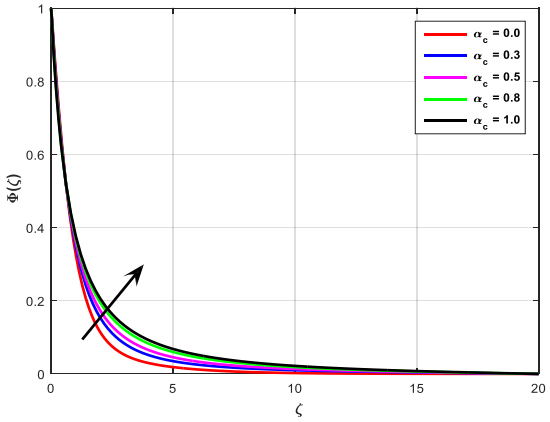

Figure-2c. Variations in $\Phi(\zeta)$ caused by α_c.

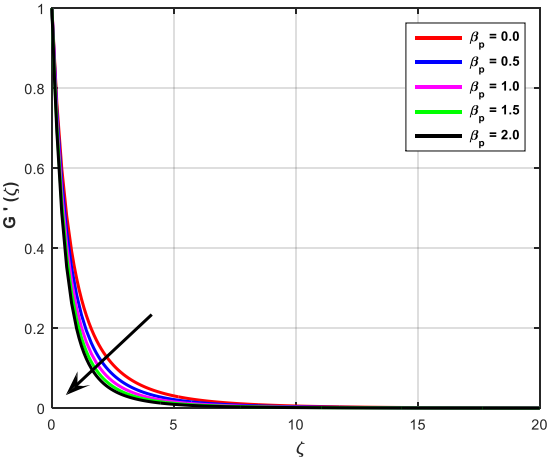

Figure-3a. Variations in $G'(\zeta)$ caused by β_p.

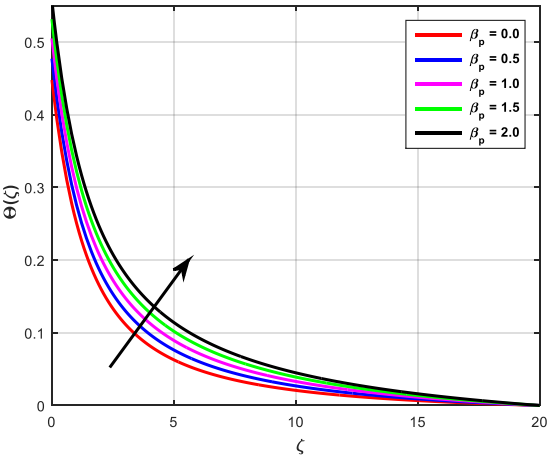

Figure-3b. Variations in $\theta(\zeta)$ caused by β_p.

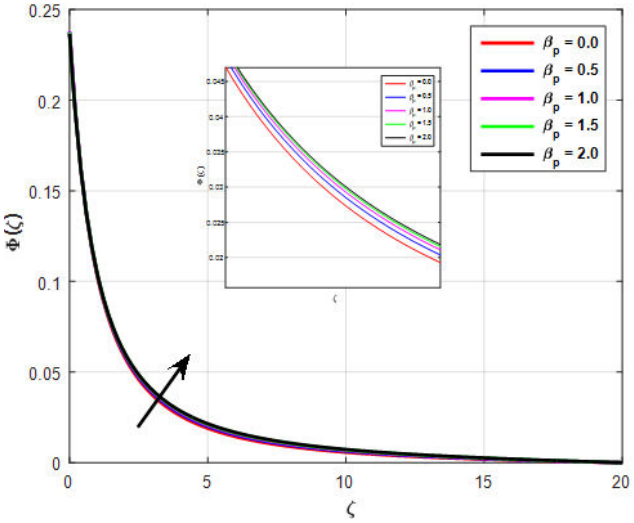

Figure-3c. Variations in $\Phi(\zeta)$ caused by β_p.

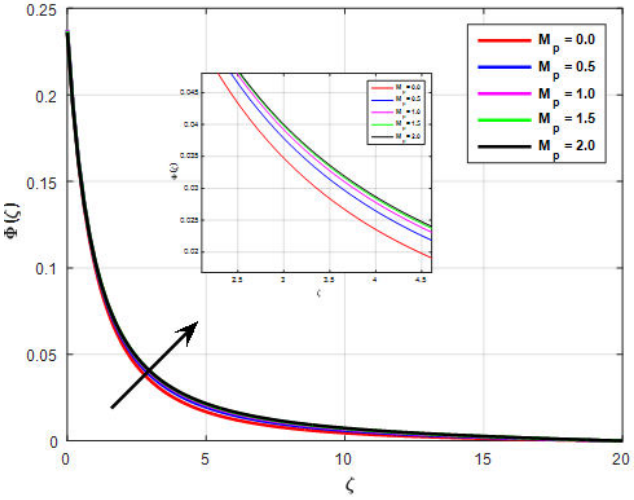

Figure-4c. Variations in $\Phi(\zeta)$ caused by M_p.

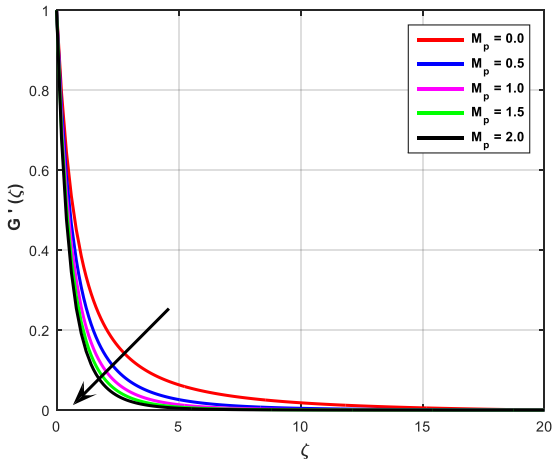

Figure-4a. Variations in $G'(\zeta)$ caused by M_p.

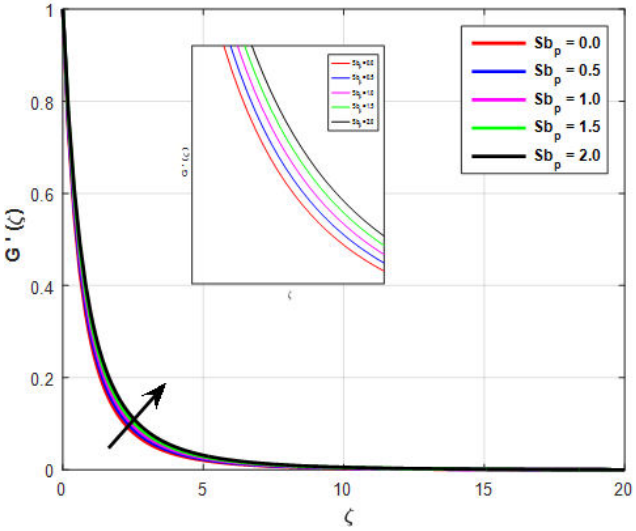

Figure-5a. Variations in $G'(\zeta)$ caused by Sb_p.

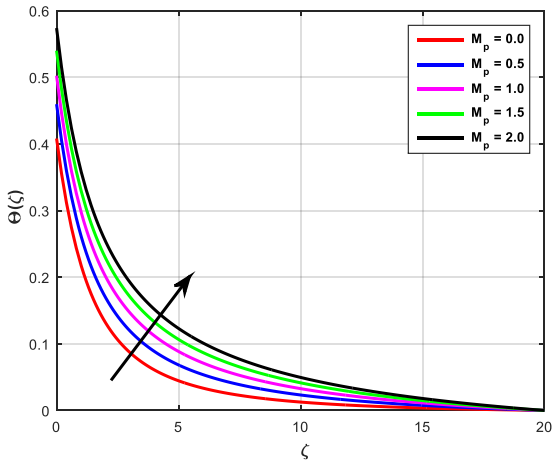

Figure-4b. Variations in $\theta(\eta)$ caused by M_p.

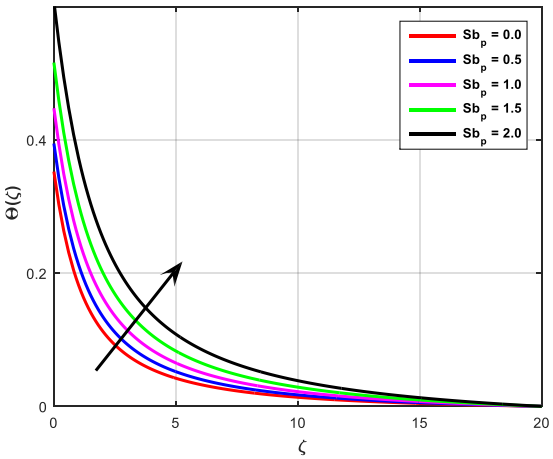

Figure-5b. Variations in $\theta(\eta)$ caused by Sb_p.

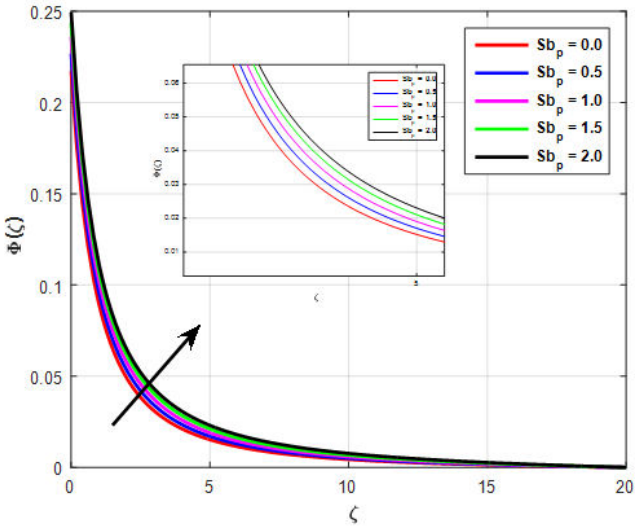

Figure-5c. Variations in $\Phi(\zeta)$ caused by Sb_p.

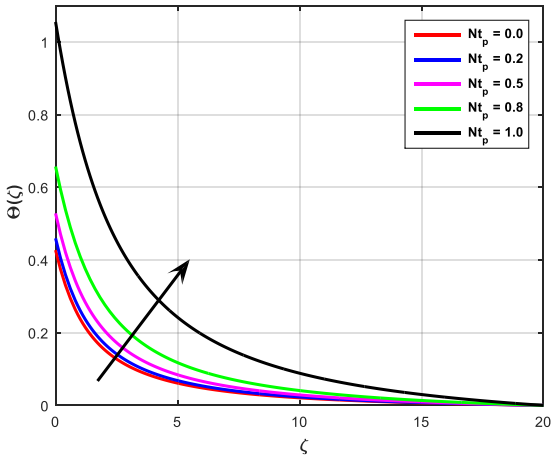

Figure-6a. Variations in $\theta(\zeta)$ caused by Nt_p.

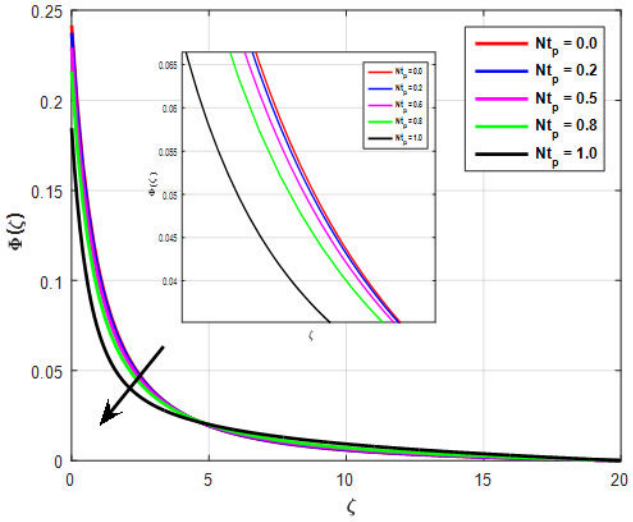

Figure-6b. Variations in $\Phi(\zeta)$ caused by Nt_p.

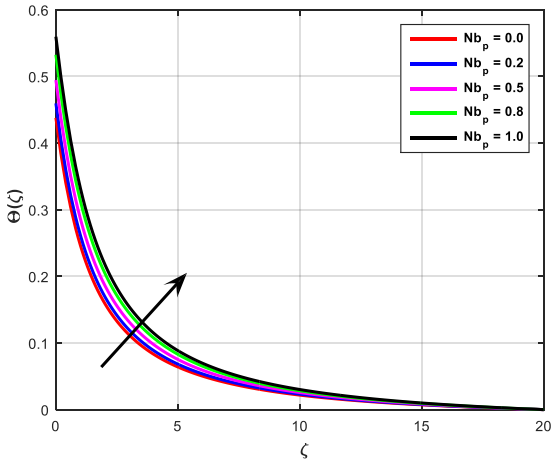

Figure-7a. Variations in $\theta(\zeta)$ caused by Nb_p.

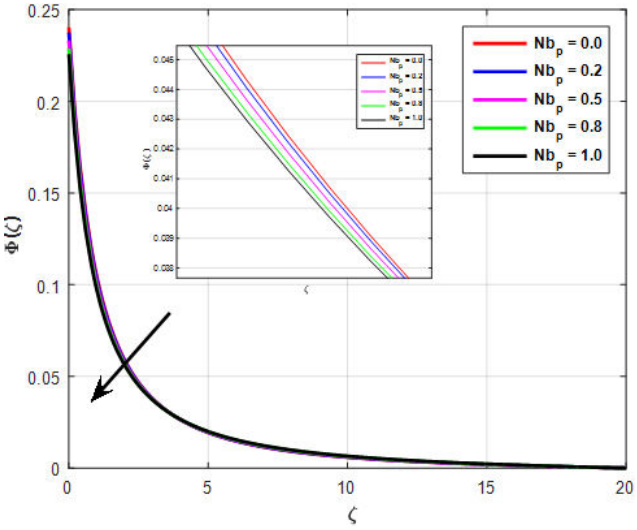

Figure-7b. Variations in $\Phi(\zeta)$ caused by Nb_p.

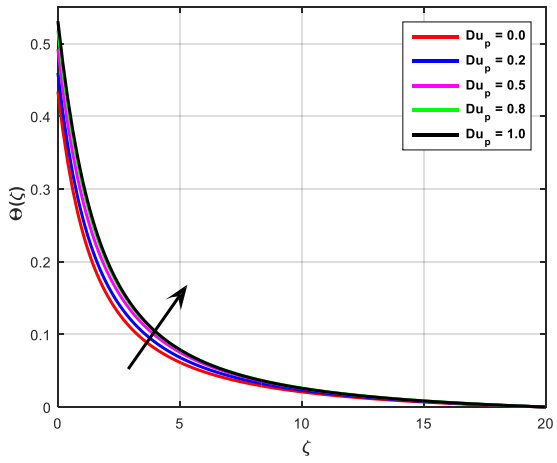

Figure-8a. Variations in $\theta(\zeta)$ caused by Du_p.

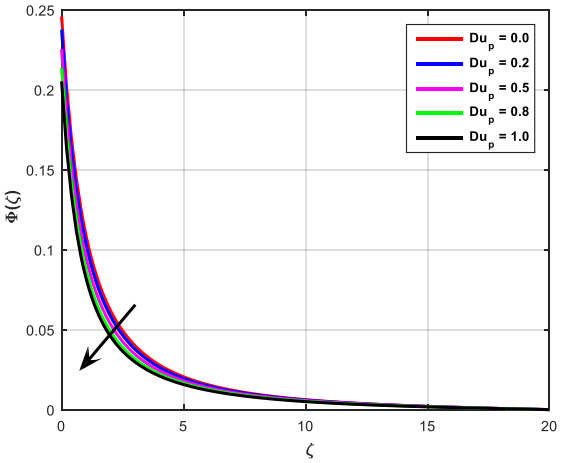

Figure-8b. Variations in $\Phi(\zeta)$ caused by Du_p.

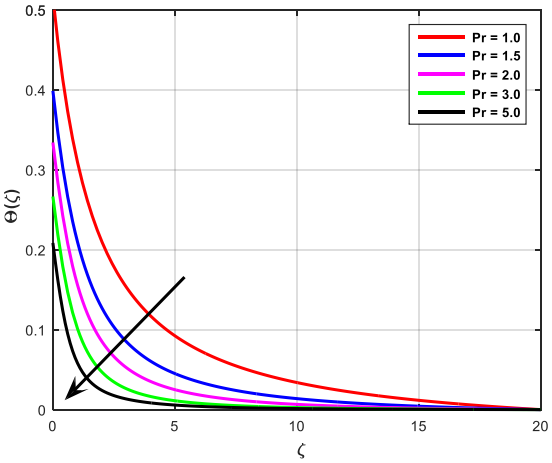

Figure-10. Variations in $\theta(\zeta)$ caused by $\Pr$.

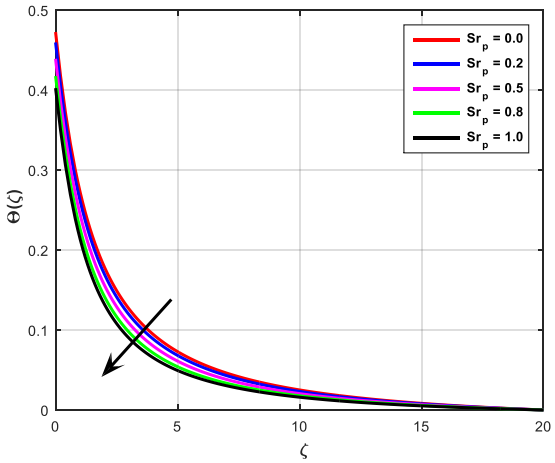

Figure-9a. Variations in $\theta(\zeta)$ caused by Sr_p.

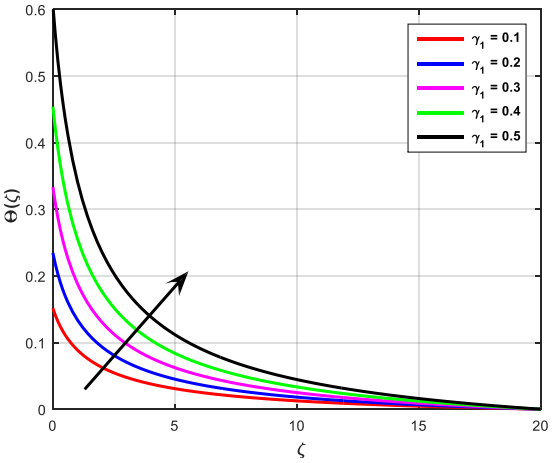

Figure-11. Variations in $\theta(\zeta)$ caused by γ_1.

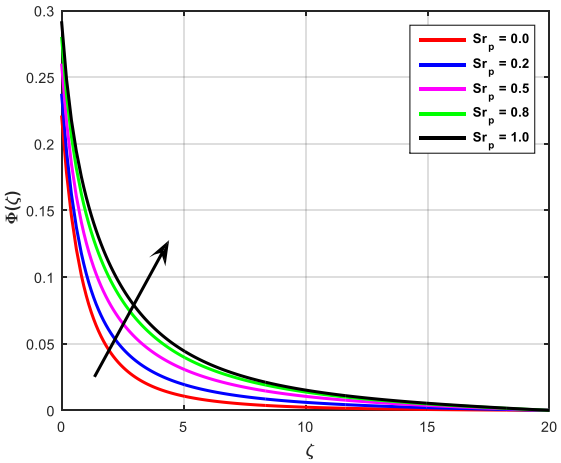

Figure-9b. Variations in $\Phi(\zeta)$ caused by Sr_p.

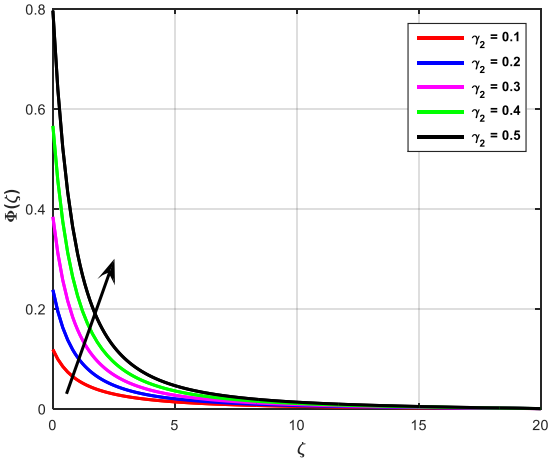

Figure-12. Variations in $\Phi(\zeta)$ caused by γ_2.

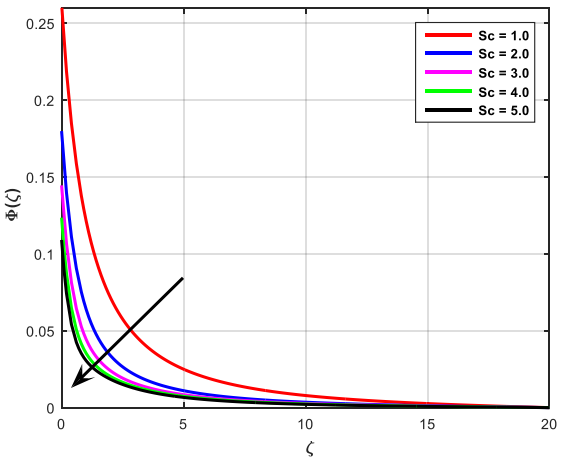

Figure-13. Variations in $\Phi(\zeta)$ caused by Sc.

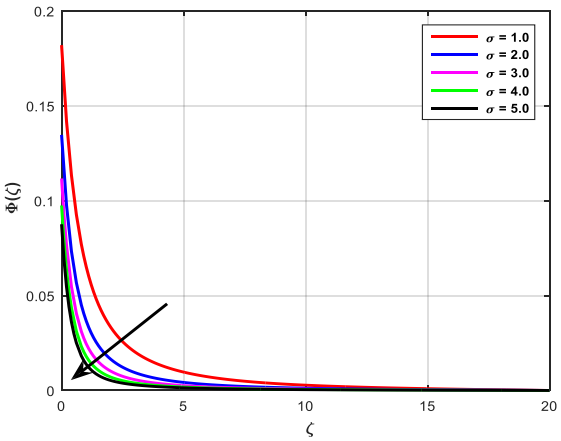

Figure-14. Variations in $\Phi(\zeta)$ caused by σ.

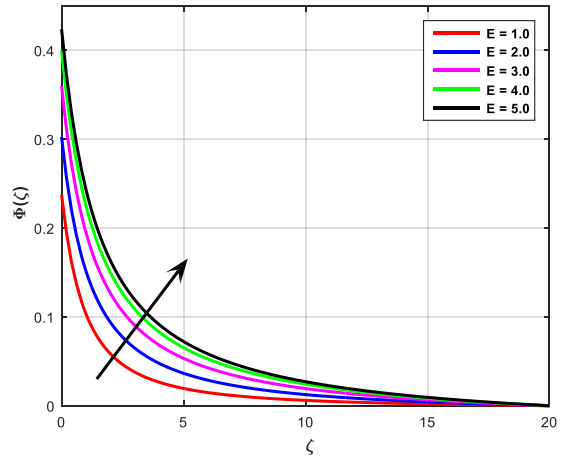

Figure-15. Variations in $\Phi(\zeta)$ caused by E.

Nomenclature	
a_o – radius of cylinder	θ - Non-dimensional temperature
l -reference length	Sb_p - Stefan blowing parameter
G – Dimensionless stream function	R - Radiation parameter
z -axial coordinate	Pr – Prandtl number
r -radial coordinate	C - Temperature of the fluid
B_0 -strength of magnetic field	C_w - Concentration of the surface
u_w - Stretching velocity	C_∞ - Ambient fluid Concentration
β_p -Deborah parameter	q_m –wall mass flux
M_p -Magnetic parameter	Du_p -mass flux relaxation time
c_p – Specific heat at constant pressure	Φ - Non-dimensional Concentration
T - Temperature of the fluid	Sc – Schmidt number
T_w - Temperature of the surface	Sr_p -soret parameter
T_∞ - Ambient fluid temperature	w – Condition at the surface
α - thermal diffusivity	∞ - Condition at infinity
k - Thermal conductivity	ζ – Similarity variable
μ - Thermal viscosity	Re_r - Local Reynolds number
ρ -Fluid density	C_f - Skin friction coefficient
$\nu = \mu/\rho$ - Kinematic viscosity of the fluid	Nu_r -Local Nusselt number
q_w - Surface heat flux	‘ – order of derivative

REFERENCES

[1] Maxwell JC. 1881. A treatise on electricity and magnetism, (Vol. 1). Clarendon Press.

[2] Mukhopadhyay S. 2012. Heat transfer analysis of the unsteady flow of a Maxwell fluid over a stretching surface in the presence of a heat source/sink. Chin Phys. Lett. 29: 054703. doi:10.1088/0256-307x/29/5/054703

[3] Yang X, Lu T, Kim T. 2013. Thermal stretching in two-phase porous media: Physical basis for Maxwell

model. Theor Appl. Mech. Lett. 3: 021011. doi:10.1063/2.1302111

[4] Ramzan M, Bilal M, Chung JD, Farooq U. 2016. Mixed convective flow of Maxwell nanofluid past a porous vertical stretched surface-An optimal solution. Results Phys. 6: 1072-9. doi:10.1016/j.rinp.2016.11.036

[5] Irfan M, Khan M, Khan WA, Ayaz M. 2018. Modern development on the features of magnetic field and heat sink/source in Maxwell nanofluid subject to convective heat transport. Phys. Lett A. 382: 1992-2002. doi:10.1016/j.physleta.2018.05.008

[6] MHD Flow of Thermally Radiative Maxwell Fluid Past a Heated Stretching Sheet with Cattaneo-Christov Dual Diffusion K. Loganathan ,1 Nazek Alessa, 2 Ngawang Namgyel, 3 and T. S. Karthik4 Journal of Mathematics Volume 2021, Article ID 5562667, 10 pages https://doi.org/10.1155/2021/5562667

[7] Sajid Shah, Naila Rafiq, Farah Aini Abdullah, S. M. Atif, Muhammad Abbas. 2022. Slip and radiative effects on MHD Maxwell nanofluid with non-Fourier and non-Fick laws in a porous medium, Case Studies in Thermal Engineering, Vol. 30, https://doi.org/10.1016/j.csite.2022.101779.

[8] AL Nuwairan, M.; Hafeez,A.; Khalid, A.; Souayeh, B.; Alfadhli N., Alnaghmosh A. 2022. Flow of Maxwell Fluid with Heat Transfer through Porous Medium with Thermophoresis Particle Deposition and Soret-Dufour Effects: Numerical Solution. Coatings, 12, 1567. https://doi.org/10.3390/coatings12101567

[9] Crane, L. J. 1975. Boundary layer flow due to a stretching cylinder. Journal of Applied Mathematics and Physics (ZAMP) 26, 619-622. https://doi.org/10.1007/BF01594034

[10] C Y Wang. 1988. Fluid flow due to a stretching cylinder The Physics of Fluids. 31, 466. https://doi.org/10.1063/1.866827Phys. Fluids. 31, 466.

[11] Wang C. Y. and C.-O. Ng. 2011. Slip flow due a stretching cylinder. Int. J. Nonlinear Mech. 46, 1191-1194

[12] J. H. Markin, N. Najib, N. Bachok, A. Ishak, I. Pop. 2017. Stagnation-point flow and heat transfer over an exponentially stretching/shrinking cylinder, J. Taiwan Inst. Chem. Eng. 74: 65-72.

[13] T. Hayat, M. Ijaz Khan, M. Waqas, A. Alsaedi. 2017. Effectiveness of magnetic nanoparticles in radiative flow of Eyring-Powell fluid. Journal of Molecular Liquids, 231: 126-133, ISSN 0167-7322, https://doi.org/10.1016/j.molliq.2017.01.076.

[14] K. U. Rehman, A. Qaiser, M. Y. Malik and U. Ali. 2017. Numerical communication for MHD thermally stratified dual convection flow of Casson fluid yields by stretching cylinder. Chinese Journal of Physics. 55, 1605-1614. https://doi.org/10.1016/j.cjph.2017.05.002

[15] Islam S., Khan A., Kumam P. *et al.* 2020. Radiative mixed convection flow of maxwell nanofluid over a stretching cylinder with joule heating and heat source/sink effects. *Sci Rep* 10, 17823. https://doi.org/10.1038/s41598-020-74393-2

[16] Hayat T, Shehzad SA, Alsaedi A. 2012. Soret and Dufour effects on MHD flow of Casson fluid. Applied Mathematics and Mechanics. 33: 1301-1312. https://doi.org/10.1007/s10483-012-1623-6

[17] Mahdy A. 2015. Heat Transfer and Flow of a Casson Fluid Due to a Stretching Cylinder with the Soret and Dufour Effects. J Eng Phys Thermophy 88, 928-936. https://doi.org/10.1007/s10891-015-1267-6

[18] Pal D, Mandal G, Vajravalu K. 2016. Soret and Dufour effects on MHD convective-radiative heat and mass transfer of nanofluids over a vertical non-linear stretching/shrinking sheet. Applied Mathematics and Computation. 287-288. https://doi.org/10.1016/j.amc.2016.04.037

[19] Uhammad Ijaz Khan, Muhammad Waqas, Tasawar Hayat, Ahmed Alsaedi. 2017. Soret and Dufour effects in stretching flow of Jeffrey fluid subject to Newtonian heat and mass conditions, Results in Physics, 7: 4183-4188, ISSN 2211-3797, https://doi.org/10.1016/j.rinp.2017.10.011.

[20] Jagan K., Sivasankaran S., Bhuvaneswari M., Rajan S. and Makinde O. D. 2018. Soret and Dufour Effect on MHD Jeffrey Nanofluid Flow towards a Stretching Cylinder with Triple Stratification, Radiation and Slip. Defect and Diffusion Forum, 387, 523-533. https://doi.org/10.4028/www.scientific.net/ddf.387.523

[21] Jagan K, Sivasankaran S. 2022. Soret and Dufour and Triple Stratification Effect on MHD Flow with Velocity Slip towards a Stretching Cylinder. Mathematical and Computational Applications. 27(2): 25. https://doi.org/10.3390/mca27020025

[22] Narayanaswamy MK, Kandasamy J, Sivanandam S. 2022. Impacts of Stefan Blowing on Hybrid Nanofluid Flow over a Stretching Cylinder with Thermal Radiation and Dufour and Soret Effect. Mathematical and Computational Applications. 27(6): 91. https://doi.org/10.3390/mca27060091

[23] B. Ahmed, F. Akbar, A. Ghaffari, Sami Ullah Khan, M. Ijaz Khan and Y. Dharmendar Reddy. 2022. Soret and Dufour aspects of the third-grade fluid due to the stretching cylinder with the Keller box approach, Waves in Random and Complex Media, DOI: 10.1080/17455030.2022.2085891

[24] D. B. Spalding. 1954. Mass transfer in laminar flow, Proc. R. Soc. Lond. Ser. Math. Phys. Sci. 221: 78-99.

[25] T. Fang, W. Jing. 2014. Flow, heat, and species transfer over a stretching plate considering coupled Stefan blowing effects from species transfer, Commun. Nonlinear Sci. Numer. Simul. 19: 3086-3097.

[26] S. R. Alamri, N. Ellahi, N. Shehzad, A. Zeeshan. 2019. Convective radiative plane Poiseuille flow of nanofluid through porous medium with slip: an application of Stefan blowing, J. Mol. Liquid. 273: 292-304.

[27] Amirsom N. A., Uddin M. J., Ismail A. IMd. 2019. MHD boundary layer bio nano convective non-Newtonian flow past a needle with Stefan blowing: Amirsom *et al.* Heat Transf. Asian Res. 48(2): 727-743. https://doi.org/10.1002/htj.21403

[28] T. A. Yusuf, F. Mabood. 2020. Slip effects and entropy generation on inclined MHD flow of Williamson fluid through a permeable wall with chemical reaction via DTM, Math. Modell. Eng. Probl. 7: 1-9.

[29] Ali B., Hussain S., Abdal S., Mehdi M.M. 2021. Impact of Stefan blowing on thermal radiation and Cattaneo-Christov characteristics for nanofluid flow containing microorganisms with ablation/accretion of 123 Int. J. Appl. Comput. Math. 7: 109 Page 15 of 16, 109.

[30] Zaib A., Rashidi M.M., Chamkha A.J. and Bhattacharyya K. 2017. Numerical solution of second law analysis for MHD Casson nanofluid past a wedge with activation energy and binary chemical reaction. International Journal of Numerical Methods for Heat & Fluid Flow. 27(12): 2816-2834, https://doi.org/10.1108/HFF-02-2017-0063

[31] Rekha M. B., Sarris, I. E., Madhukesh, J. K., Raghunatha, K. R., Prasannakumara B. C. 2022. Activation Energy Impact on Flow of AA7072-AA7075/Water-Based Hybrid Nanofluid through a Cone, Wedge and Plate. Micromachines. 13, 302. https://doi.org/10.3390/mi13020302.

[32] Reddy SC, Asogwa KK, Yassen MF, Adnan, Iqbal Z, M-Eldin S, Ali B and KM S. 2022. Dynamics of MHD second grade nanofluid flow with activation energy across a curved stretching surface. Front. Energy Res. 10:1007159.doi: 10.3389/fenrg.2022.1007159

[33] Khan U., Zaib A., Ishak A. 2023. Impact of Thermal and Activation Energies on GlauertWall Jet (WJ) Heat and Mass Transfer Flows Induced by ZnO-SAE50 Nano Lubricants with Chemical Reaction: The Case of Brinkman-Extended Darcy Model. Lubricants, 11, 22.https://doi.org/10.3390/lubricants11010022.

[34] Khan A, Iqbal Z, Ahammad NA, Sidi MO, Elattar S, Awad S, Yousef ES and Eldin SM. 2023. Bio convection Maxwell nanofluid flow over a stretching cylinder influenced by chemically reactive activation energy surrounded by a permeable medium. Front. Phys. 10: 1065264. doi: 10.3389/fphy.2022.1065264

[35] Zafar S.S., Alfaleh A., Zaib A., Ali F., Faizan M., Abed A.M., Elattar S., Khan M.I. 2023. Simulation of Prandtl Nanofluid in the Mixed Convective Flow of Activation Energy with Gyrotactic Microorganisms: Numerical Outlook Features of Micro-Machines. Micromachines. 14, 559. https://doi.org/10.3390/mi14030559.

[36] Zeeshan Ahammad N. A., Shah N. A., Chung J. D., Attaullah Rasheed H. U. 2023. Analysis of Error and Stability of Nanofluid over Horizontal Channel with Heat/Mass Transfer and Nonlinear Thermal Conductivity. Mathematics, 11, 690. https://doi.org/10.3390/math11030690.

[37] Abel MS, Tawade JV, Nandeppanavar MM. 2012. MHD flow and heat transfer for the upper-convected Maxwell fluid over a stretching sheet. Meccanica. 47: 385-93. doi:10.1007/s11012-011-9448-7

[38] Megahed AM. 2013. Variable fluid properties and variable heat flux effects on the flow and heat transfer in a non-Newtonian Maxwell fluid over an unsteady stretching sheet with slip velocity. Chin Phys B. 2013: 094701. doi:10.1088/1674-1056/22/9/094701

[39] Waqas M., Khan MI, Hayat T, Alsaedi A. 2017. Stratified flow of an Oldroyd-B nanofluid with heat generation. Results Phys. 7: 2489-96.

[40] Irfan M., Khan M., Khan WA. 2019. Impact of homogeneous–heterogeneous reactions and non-Fourier heat flux theory in Oldroyd-B fluid with variable conductivity. J Braz Soc Mech Sci Eng. 41: 135. doi: 10.1007/s40430-019-1619-9.

[41] Fang T., Zhang J., Yao S. 2009. Slip MHD viscous flow over a stretching sheet - an exact solution. Commun Nonlinear Sci Numer Simul. 14: 3731-7. doi:10.1016/j.cnsns.2009.02.012

[42] Fathizadeh M, Madani M, Khan Y, Faraz N, Yıldırım A, Tutkun S. 2013. An effective modification of the homotopy perturbation method for MHD viscous flow over a stretching sheet. J King Saud Univ - Sci. 25: 107-13. doi:10.1016/j.jksus.2011.08.003

[43] Hayat T, Shafiq A, Alsaedi A. 2015. MHD axisymmetric flow of third grade fluid by a stretching cylinder. Alexandria Eng J. 54: 205-12. doi:10.1016/j.aej.2015.03.013

[44] Ahmed A, Khan M, Irfan M, Ahmed J. 2020. Transient MHD flow of Maxwell nanofluid subject to nonlinear thermal radiation and convective heat transport. Appl. Nanoscience. 10: 5361-73. doi:10.1007/s13204-020-01375-1

[45] Ahmed A., Alhowaity S., Ghoneim ME, Gamaoun F., Tag-eldin E., Yassen MF and Sarfraz M. 2022. Material and wave relaxation phenomena effects on the rheology of Maxwell nanofluids. Front. Phys. 10:1005056.doi: 10.3389/fphy.2022.1005056

[46] Grubka L. J., Bobba K. M. 1985. Heat transfer characteristics of a continuous, stretching surface with variable temperature. ASME J Heat Transf. 107, 248-25.

[47] Ali M. E. 1994. Heat transfer characteristics of a continuous stretching surface. *Heat Mass Transfer.* 29, 227-234.

[48] Chen C. H. 1998. Laminar mixed convection adjacent to vertical, continuously stretching sheets. Heat Mass Transfer. 33,471-476.

[49] Anuar Ishak. 2010. Thermal boundary layer flow over a stretching sheet in a micropolar fluid with radiation effect, *Meccanica* 45, 367-373, DOI 10.1007/s11012-009-9257-4.

[50] W. A. Khan, I. Pop. 2010. Boundary-layer flow of a nanofluid past a stretching sheet, International Journal of Heat and Mass Transfer, 53(11-12): 2477-2483, ISSN 0017-9310, https://doi.org/10.1016/j.ijheatmasstransfer.2010.01.032.

[51] C. Y. Wang. 1989. Free convection on a vertical stretching surface, J. Appl. Math. Mech. (ZAMM). 69: 418-420.

[52] R.S.R. Gorla, I. Sidawi. 1994. Free convection on a vertical stretching surface with suction and blowing, Appl. Sci. Res. 52: 247-257.

[53] M. Khan, M. Irfan, W. A. Khan, Impact of heat source/sink on radiative heat transfer to Maxwell nanofluid subject to revised mass flux condition, Results in Physics, 9: 851-857, ISSN 2211-3797, https://doi.org/10.1016/j.rinp.2018.03.034.

[54] M. Irfan, M. Khan, W. A. Khan, M. Ayaz. 2018. Modern development on the features of magnetic field and heat sink/source in Maxwell nanofluid subject to convective heat transport, Physics Letters A, 382(30): 1992-2002, ISSN 0375-9601, https://doi.org/10.1016/j.physleta.2018.05.008.